Detection via simultaneous trajectory estimation and long time integration

Kimin Kim, *Student Member, IEEE*, Murat Üney, *Member, IEEE*,
and Bernard Mulgrew, *Fellow, IEEE*

Abstract

In this work, our focus is on the detection of manoeuvring small objects with radars. Such objects induce low signal to noise ratio (SNR) reflections in the received signal. We consider both co-located and separated transmitter/receiver pairs, i.e., mono-static and bi-static configurations, respectively, as well as multi-static settings involving both types. We propose a detection approach which is capable of coherently integrating these reflections within a coherent processing interval (CPI) in all these configurations and continuing integration for an arbitrarily long time across consecutive CPIs. We estimate the complex value of the reflection coefficient for integration while simultaneously estimating the object trajectory. Compounded with this is the estimation of the unknown time reference shift of the separated transmitters necessary for coherent processing. Detection is made by using the resulting integration value in a Neyman-Pearson test against a constant false alarm rate threshold. We demonstrate the efficacy of our approach in a simulation example with a very low SNR object which cannot be detected with conventional techniques.

Index Terms

radar detection, coherent integration, non-coherent integration, bi-static radar, multi-static radar, target tracking, synchronisation.

I. Introduction

Detection of manoeuvring and small objects with radars is a challenging task [1], and, a highly desirable capability in surveillance applications [2]. Radars emit modulated pulses toward

This work was supported by the Engineering and Physical Sciences Research Council (EPSRC) grant EP/K014277/1, and, the MOD University Defence Research Collaboration (UDRC) in Signal processing.

K. Kim, M. Üney, and B. Mulgrew are with Institute for Digital Communications, School of Engineering, the University of Edinburgh, Edinburgh, EH9 3JL, U.K. (e-mail:{K.Kim, M.Uney, B.Mulgrew}@ed.ac.uk).

a surveillance region, and, collect reflected versions of the transmitted waveforms from objects in this area. Small objects induce low signal-to-noise ratio (SNR) signals at the radar receiver. The decision on object presence is made by testing the hypothesis that the received signal contains reflections against the noise only signal hypothesis after the front-end input is filtered with a system response matching the probing waveform, which is known as the matched filter (MF) [3].

In order to detect low SNR objects, multiples of such pulse returns (i.e., multiple measurements) need to be considered as each reflection is at a level similar to the noise background. The sufficient statistics of multiple pulse returns are found by summing the associated reflection coefficients across them, which is referred to as pulse integration [3, Chp.8]. This process is applied on the sampled outputs of the MF stage. These samples correspond to, in effect, resolution bins in an equally divided range-bearing and doppler space. Conventional integration methods such as coherent and non-coherent integration integrate pulse returns in the same range-bearing and doppler bins across time. When objects manoeuvre, however, these reflections follow a trajectory across these bins, and, these methods fail to collect evidence on object existence for a long time due to not taking into account this trajectory. On the other hand, longer integration time provides higher probability of detection for a given false alarm rate, in principle.

One possible solution to long time integration in the case of object manoeuvres is to design filters with long time responses matching multiple pulse returns along a selection of possible trajectories [4]. The number of filters required in this approach easily becomes impractically excessive with increasing integration time, however. An alternative approach is to employ a dynamic programming perspective and use a regular probing pulse MF to integrate its outputs along a trajectory estimated simultaneously which corresponds to, in a sense, online synthesis of long time MFs adaptively. Trajectory estimation using outputs of a pulse MF is often referred to as track-before-detect (see, for example, [5], [6]). The sample that corresponds to the true object kinematic is a complex value that is a sum of the reflection coefficient and background noise [7] [1]. Most track-before-detect algorithms use averaged models that specify statistics of the modulus of the MF output. The detection performance can be improved by also taking into account the phase of the data samples [8].

[1]In general, the received reflection is characterised by a complex reflection coefficient and the reflector's kinematics such as location (equivalently the time of flight) and velocity (equivalently doppler shift) [7, Chp.2]. Sampled MF outputs are used to form a radar data-cube that maps range-bearing and doppler bins to a complex MF output sample [3]. We refer to the sample in this cube that corresponds to the true object kinematic.

The best achievable detection performance is obtained by coherent processing [3], in which one needs to estimate the complex reflection coefficient from the complex values of the MF outputs the latter of which are processed by the aforementioned algorithms. This corresponds to using a non-averaged model in which the reflection coefficient is a random variable that remains the same during what is known as a coherent processing interval (CPI), and, is generated randomly for consecutive CPIs [7]. This is challenging partly because estimation of this quantity with a reasonable accuracy requires more samples than one can collect at the pulse-width sampling rate in a coherent processing interval (CPI) [9]. For example, [10] performs coherent processing and integration within a CPI, however, with a very high sampling rate that yields an extensive number of samples in a pulse interval.

In [11], we demonstrated that this can be remedied using a phased array receiver structure. In particular, we assume a uniform linear array (ULA) receiver and sample its elements with a pulse-width period. Then, we use these complex measurements for estimating the complex reflection coefficients in consecutive CPIs. Simultaneously, we perform trajectory estimation with an arbitrary target motion model, and, use the estimated coefficients in pulse integration which can be continued for an arbitrarily long time. The integrated value is then tested against a constant false alarm rate (CFAR) threshold for declaring the existence or otherwise of an object in a Neyman-Pearson sense. The coherency of processing is ensured by the knowledge of the transmitter characteristics and synchronisation with the receiver so that there is no unknown phase shift in the received reflections. In [12], we extend this approach for separated transmitter/receiver pairs, i.e., bi-static channels, with an unknown time reference shift. In particular, we recover the synchronisation term by diverting simultaneous beams towards the tested point of detection and the remote transmitter thereby relaxing the commonly used assumption that the remote transmitters and the local receiver are synchronised (see, e.g., [13], [14]).

In this work, we provide a complete exposition of our long time integration and trajectory estimation approach in mono-static and bi-static configurations, and, introduce a novel solution for the multi-static case in which both mono-static and bi-static channels exist. In particular, we consider the system structure in Fig. 1 where there are multiple transmitters using mutually orthogonal waveforms. The receiver is a ULA and has the full knowledge of the transmission characteristics except the time reference shift of the separately located transmitters. The front-end signals at the receive elements are the superposition of noise, signals from direct channels, and, reflections from objects.

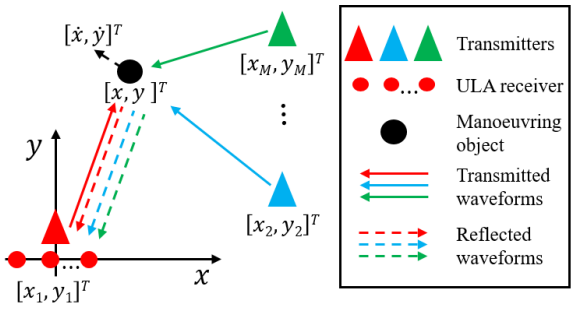

Fig. 1: Problem scenario: M transmitters and a ULA receiver are to detect a small object located at $[x,y]^T$ with velocity $[\dot{x},\dot{y}]^T$ inducing a low SNR signal onto the receiver elements.

We use a Markov state-space model for the object state which consists of location and velocity variables. The measurement model of this state space model involves the radar ambiguity function parametrised on the aforementioned reflection coefficients. These coefficients are estimated using a maximum likelihood approach within Bayesian filtering recursions for state trajectory estimate. For synchronisation, we employ techniques for parameter estimation in state space models, and, in effect, use the object trajectory estimated in the mono-static channel to find the respective time reference shifts in the bi-static channels. This removes the constraint on the omni-directionality of transmitters for facilitating coherent processing in the bi-static only case.

The proposed algorithm enables us to collect the entire evidence of object existence at the receiver by i) performing coherent integration in both mono-static and bi-static channels within a CPI, ii) non-coherently integrating across different (non-coherent) channels, e.g., local mono-static and remote bi-static channels, and, iii) continuing integration for an arbitrarily long interval that contains many CPIs. As a result, this approach enables us to detect manoeuvring and low SNR objects which cannot be detected using other techniques.

This article is organised as follows: Section II gives details of the problem scenario and introduces the mathematical statement of the problem. In Section III, we discuss trajectory estimation with the array measurements and derive the maximum-likelihood estimator for the complex reflection coefficients given the estimated trajectory. Then, we introduce synchronisation approaches for bi-static only and multi-static configurations. The proposed detection algorithm is demonstrated in Section VI through an example scenario in which a manoeuvring very low SNR object is to be detected. Finally, we conclude in Section VII.

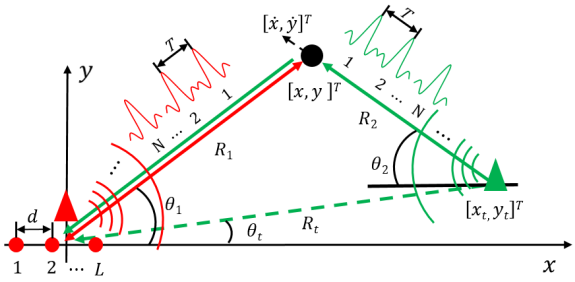

Fig. 2: Geometry of the problem scenario: One transmitter co-located with a ULA receiver and another placed in a separate location on the 2D Cartesian plane. Both polar and Cartesian coordinate variables are depicted. Each transmitter emits N pulses in a CPI. The waveforms used are orthogonal.

II. Problem Statement

This section gives the details of the problem scenario described in Fig 1. We consider a ULA receiver and introduce notation for $M = 2$ transmitters for the sake of simplicity, but, the discussion can easily be extended for $M > 2$ transmitters. In this setting, one of the transmitters is co-located with the receiver forming a mono-static pair. The second transmitter is located elsewhere and forms a bi-static pair with the receiver.

The geometry of the problem is illustrated in Fig 2. Here, each transmitter (depicted by a triangle) is assumed to be omni-directional and emits N consecutive pulses separated by a time length of T. This quantity is known as the pulse repetition interval (PRI). These pulses are reflected from an object (black circle). We assume that the reflectivity of the object remains coherent (i.e., unchanged) during the collection of these N reflections. Such a time interval is known as a CPI.

The ULA receiver (red dots) is comprised of L elements spaced with d distance. Each element collects reflected versions of the transmitted waveforms emitted by both the co-located and the separated transmitter. The corresponding channels are illustrated in Fig. 2 by coloured lines. In particular, there is i) a local (mono-static) channel (red line), ii) a remote (bi-static) channel (green line), and, iii) a direct channel from the remote transmitter (green dashed line).

A. Spatio-temporal signal model

We consider the narrowband signal models for the aforementioned three channels [15] at the ULA receiver. Let us denote the object kinematic state by $X = [x, y, \dot{x}, \dot{y}]^T$, where $[x, y]^T$ is

the location, $[\dot{x}, \dot{y}]^T$ is the velocity, and $(\cdot)^T$ denotes the transpose of its input argument. The corresponding signal can be expressed as a combination of a spatial steering vector $s_s(\theta)$ and a temporal vector $s_t(r, \omega_d)$, where θ, r, and ω_d denote the angle of arrival, the time of flight, and the doppler angular frequency, respectively.

The angle of arrival values for these channels at the receiver are given by

$$\theta_1 = \arctan\left(\frac{y}{x}\right) \quad \text{and} \quad \theta_t = \arctan\left(\frac{y_t}{x_t}\right), \tag{1}$$

where θ_1 is the angle of arrival for the local and the remote channels and θ_t is the angle of arrival for the direct channel.

The values for time of flight are found as

$$r_1 = \frac{2R_1}{c}, r_2 = \frac{R_1 + R_2}{c}, \text{and } \; r_t = \frac{R_t}{c}, \tag{2}$$

where r_1, r_2, and r_t are the time of flight for the local, the remote, and the direct channels, respectively and c is the speed of light in $\mathrm{m/s}$. Here, $R_1 = \sqrt{x^2 + y^2}$, $R_2 = \sqrt{(x - x_t)^2 + (y - y_t)^2}$, and $R_t = \sqrt{x_t^2 + y_t^2}$ are the range components of the reflector in the local polar coordinate systems shown in Fig 2.

The doppler angular frequencies of the local and the remote channels are found as

$$\begin{aligned} \omega_{d_1} &= \frac{4\pi}{\lambda_c}\left(\dot{x}\cos(\theta_1) + \dot{y}\sin(\theta_1)\right), \quad \text{and} \\ \omega_{d_2} &= \frac{2\pi}{\lambda_c}\left(\dot{x}(\cos(\theta_1) + \cos(\theta_2)) + \dot{y}(\sin(\theta_1) + \sin(\theta_2))\right), \end{aligned} \tag{3}$$

respectively. Here, λ_c is the carrier wavelength given by $\lambda_c = c/f_c$ and θ_2 is the angle in Fig 2 given by $\theta_2 = \arctan\big((y - y_t)/(x - x_t)\big)$.

The temporal vector $s_t\left(r, \omega_d\right)$ with N pulses is found as

$$s_t\left(r, \omega_d\right) = \exp\left(-j\omega_c r\right) \times \Big[1, \exp\left(j\omega_d T\right), \ldots, \exp\left(j\omega_d (N-1)T\right)\Big]^T, \tag{4}$$

where T is the pulse repetition interval (PRI) and ω_c is the carrier angular frequency given by $\omega_c = 2\pi f_c$.

The spatial steering vector $s_s(\theta)$ is characterised by the geometry of the ULA receiver with L elements and is found as

$$s_s(\theta) = \left[1, \exp\left(-j\omega_c \frac{d}{c}\sin\theta\right), \ldots, \exp\left(-j\omega_c (L-1)\frac{d}{c}\sin\theta\right)\right]^T, \tag{5}$$

where $d = \lambda_c/2$ is the internal element spacing in the ULA receiver.

After substituting the values for the angel of arrival, the time of flight, and the doppler angular frequency in (4) and (5), the forward signal models are given by combining the spatial steering and the temporal vectors i.e.,

$$\begin{aligned} s_z(\theta_1, r_1, \omega_{d_1}) &= s_s(\theta_1) \otimes s_t\left(r_1, \omega_{d_1}\right) \quad \text{and} \\ s_y(\theta_1, r_2 + \Delta t, \omega_{d_2}) &= s_s(\theta_1) \otimes s_t\left(r_2 + \Delta t, \omega_{d_2}\right), \end{aligned} \tag{6}$$

where $s_z(\cdot) \in \mathbb{C}^{LN\times 1}$ and $s_y(\cdot) \in \mathbb{C}^{LN\times 1}$ represent the noise free signals received in the local and the remote channels, respectively, Δt denotes the unknown time shift (i.e., the synchronisation term of the remote channel at the receiver), and $\otimes$ denotes the Kronecker product operator.

Similarly, the forward signal model in the direct channel is expressed as

$$s_d(\theta_t, r_t + \Delta t) = s_s(\theta_t) \otimes s_t\left(r_t + \Delta t, 0\right). \tag{7}$$

Detection is made by searching the reflections in sampled versions of the received signals after a matched filter. In particular, we use a bank of two orthogonal matched filters which match the probing waveforms emitted by two transmitters (which, in general, would be M filters with M transmitters [16, Chp.3]). This filter output is sampled in fast time which uniformly divides range space into range bins with Δr. Bearing space is discretised into bearing bins of $\Delta\theta$ and doppler space is also sampled into dopper bins of $\Delta\omega_d$ [3, Chp.7]. As a result, the data vectors in a CPI under the hypothesis that an object exists at $i = [i_1, i_2, i_3]^{\text{th}}$ and $j = [j_1, j_2, j_3]^{\text{th}}$ bearing-range and doppler bins with unknown complex reflection coefficients are given by

$$\begin{aligned} \mathcal{Z}(i) &= \alpha_z s_z(i_1\Delta\theta, i_2\Delta r, i_3\Delta\omega_d) + n_z(i_1\Delta\theta, i_2\Delta r, i_3\Delta\omega_d) \quad \text{and} \\ Y(j) &= \alpha_y s_y(j_1\Delta\theta, j_2\Delta r + \Delta t, j_3\Delta\omega_d) + n_y(j_1\Delta\theta, j_2\Delta r, j_3\Delta\omega_d), \end{aligned} \tag{8}$$

where $\mathcal{Z}(\cdot)$ and $Y(\cdot)$ are the measurements received in the local and the remote channels, respectively, and, α_z and α_y are the unknown complex reflection coefficients for these channels. Here, $n_z(\cdot)$ and $n_y(\cdot)$ represent independent complex Gaussian variables with all zero mean and covariances of Σ_z and Σ_y, respectively[2].

[2]Properties of general complex Gaussian covariances are explained in [17, Chp.7].

Now, we evaluate the sufficient statistics in the remote channel by time shifting the measurement $Y(j)$ in (8). An amount of time shifting $Y(j)$ is specified by the object kinematic parameters X. This version is found as

$$\begin{aligned}\mathcal{Y}(j) &= Y(j) \odot s_y(-\theta_1, -r_2, -\omega_{d_2}) \\ &= \alpha_y s_y(0, \Delta t, 0) + n_y(j) \\ &= \alpha_y s_y(\Delta t) + n_y(j),\end{aligned} \tag{9}$$

where $s_y(\cdot)$ is the noise free signal model given in (6), $j = [j_1, j_2, j_3]$ corresponds to the bearing-range and doppler bin associated with $(\theta_1, r_2, \omega_{d_2})$ of X, and $\odot$ denotes the Hadamard product operator. As a result, the data vectors to be tested for detection at the k^{th} CPI are given by combining the local and the remote channels, i.e.,

$$\begin{bmatrix}\mathcal{Z}_k(i) \\ \mathcal{Y}_k(j)\end{bmatrix} = \begin{cases} \begin{bmatrix}\alpha_{z,k} s_{z,k}(i_1\Delta\theta, i_2\Delta r, i_3\Delta\omega_d) \\ \alpha_{y,k} s_{y,k}(\Delta t)\end{bmatrix} + \begin{bmatrix}\mathrm{n}_{z,k}(i_1\Delta\theta, i_2\Delta r, i_3\Delta\omega_d) \\ \mathrm{n}_{y,k}(j_1\Delta\theta, j_2\Delta r, j_3\Delta\omega_d)\end{bmatrix}, & H_1 \text{ holds}, \\ \begin{bmatrix}\mathrm{n}_{z,k}(i_1\Delta\theta, i_2\Delta r, i_3\Delta\omega_d) \\ \mathrm{n}_{y,k}(j_1\Delta\theta, j_2\Delta r, j_3\Delta\omega_d)\end{bmatrix}, & H_0 \text{ holds}, \end{cases} \tag{10}$$

where $s_{y,k}(\Delta t)$ is given in (9), H_1 is the hypothesis that an object is located at i^{th} and j^{th} bins, and H_0 is the noise only signal hypothesis.

B. Problem definition

Our goal is to detect a low SNR object moving along the trajectory $X_{1:K}$. The decision on the presence of an object is made by using a Neyman-Pearson test [18, Chp.3]. The inputs to this test are the set of the complex measurement vectors $\{\mathcal{Z}_k(i_k), \mathcal{Y}_k(j_k)\}_{k=1:K}$ in (10), where $i_k = [i_{1,k}, i_{2,k}, i_{3,k}]$ and $j_k = [j_{1,k}, j_{2,k}, j_{3,k}]$ correspond to the bearing-range and doppler bins associated with $(\theta_k, r_k, \omega_{d_k})$ of the object sate X_k.

Given the object state $X_{1:K}$, the likelihood ratio test is defined as

$$\begin{aligned}&L(\mathcal{Z}_{1:K}(i_{1:K}), \mathcal{Y}_{1:K}(j_{1:K}) | X_{1:K}, \alpha_{z,1:K}, \alpha_{y,1:K}, \Delta t) = \\ &\prod_{k=1}^{K} \frac{l(\mathcal{Z}_k(i_k), \mathcal{Y}_k(j_k) | X_k, \alpha_{z,k}, \alpha_{y,k}, \Delta t, H = H_1)}{l(\mathcal{Z}_k(i_k), \mathcal{Y}_k(j_k) | H = H_0)} \underset{H_0}{\overset{H_1}{\gtrless}} \mathcal{T}_K,\end{aligned} \tag{11}$$

where the likelihood ratio $L(.)$ is used for the detection test at the receiver, the likelihood $l(.|H = H_1)$ represents the object existence hypothesis $H = H_1$, the likelihood $l(.|H = H_0)$ is for the noise only signal hypothesis $H = H_0$, and $\mathcal{T}_K$ is the detection threshold for K steps of integration.

The numerator at the k^{th} CPI in (11) –considering (10) – is given by

$$\begin{aligned} l(\mathcal{Z}_k(i_k), \mathcal{Y}_k(j_k)|X_k, \alpha_{z,k}, \alpha_{y,k}, \Delta t, H = H_1) &= \left(\frac{1}{\pi^{2LN}\det(\Sigma_z)\det(\Sigma_y)}\right) \\ \times \exp\Big(-\big(\mathcal{Z}_k(i_k) - \alpha_{z,k}s_{z,k}(X_k)\big)^H \Sigma_z^{-1}\big(\mathcal{Z}_k(i_k) - \alpha_{z,k}s_{z,k}(X_k)\big)\Big) \\ \times \exp\Big(-\big(\mathcal{Y}_k(j_k) - \alpha_{y,k}s_{y,k}(\Delta t)\big)^H \Sigma_y^{-1}\big(\mathcal{Y}_k(j_k) - \alpha_{y,k}s_{y,k}(\Delta t)\big)\Big), \end{aligned} \tag{12}$$

and the denominator is also found as

$$\begin{aligned} l(\mathcal{Z}_k(i_k), \mathcal{Y}_k(j_k)|H_0) &= \left(\frac{1}{\pi^{2LN}\det(\Sigma_z)\det(\Sigma_y)}\right) \\ \times \exp\Big(-\mathcal{Z}_k(i_k)^H\Sigma_z^{-1}\mathcal{Z}_k(i_k) - \mathcal{Y}_k(j_k)^H\Sigma_y^{-1}\mathcal{Y}_k(j_k)\Big), \end{aligned} \tag{13}$$

where $\mathcal{Z}_k(i_k) \in \mathcal{C}^{LN\times 1}$ and $\mathcal{Y}_k(j_k) \in \mathcal{C}^{LN\times 1}$ are the measurements in (10), LN is the length of the data vector, and $(.)^H$ denotes the Hermitian transpose of its input argument.

An explicit expression for the instantaneous likelihood ratio at the k^{th} CPI in (11) after substituting (12) and (13) is hence obtained by

$$\begin{aligned} &L(\mathcal{Z}_k(i_k), \mathcal{Y}_k(j_k)|X_k, \alpha_{z,k}, \alpha_{y,k}, \Delta t) \\ &= \exp\Big(-\big(\mathcal{Z}_k(i_k) - \alpha_{z,k}s_k(X_k)\big)^H \Sigma_z^{-1}\big(\mathcal{Z}_k(i_k) - \alpha_{z,k}s_{z,k}(X_k)\big)\Big) \\ &\times \exp\Big(-\big(\mathcal{Y}_k(j_k) - \alpha_{y,k}s_{y,k}(\Delta t)\big)^H \Sigma_y^{-1}\big(\mathcal{Y}_k(j_k) - \alpha_{y,k}s_{y,k}(\Delta t)\big)\Big) \\ &\times \exp\Big(\mathcal{Z}_k(i_k)^H\Sigma_z^{-1}\mathcal{Z}_k(i_k) + \mathcal{Y}_k(j_k)^H\Sigma_y^{-1}\mathcal{Y}_k(j_k)\Big). \end{aligned} \tag{14}$$

Now, the problem we consider involves simultaneous estimation of the object state $X_{1:K}$ and evaluation the likelihood ratio in (11) by evaluating (12)–(14) for $k = 1, 2, \cdots, K$. This also requires estimation of the complex reflection coefficients and Δt. Estimation of all these unknown parameters, and, specification of the detection threshold for a constant false alarm rate (CFAR) are explained in the rest of this article.

III. Simultaneous tracking and reflection coefficient estimation

A. Trajectory estimation using coherent returns

In this section, we consider estimation of the object trajectory $X_{1:k}$ using coherent returns during a CPI. For this purpose, we use Bayesian recursive filtering based on a Markov state space model. This filtering is given by the prediction and the update recursion:

$$p(X_k|\mathcal{Z}_{1:k-1},\mathcal{Y}_{1:k-1}) = \int p(X_k|X_{k-1})p(X_{k-1}|\mathcal{Z}_{1:k-1},\mathcal{Y}_{1:k-1})dX_{k-1} \tag{15}$$

$$p(X_k|\mathcal{Z}_{1:k},\mathcal{Y}_{1:k}) \propto p(\mathcal{Z}_k,\mathcal{Y}_k|X_k,\alpha_{z,k},\alpha_{y,k},\Delta t)p(X_k|\mathcal{Z}_{1:k-1},\mathcal{Y}_{1:k-1}) \tag{16}$$

where $p(X_k|\mathcal{Z}_{1:k},\mathcal{Y}_{1:k})$ is the posterior density function of the object state X_k, $p(X_k|X_{k-1})$ is the Markov transition density of X_k, and $p(\mathcal{Z}_k,\mathcal{Y}_k|X_k,\alpha_{z,k},\alpha_{y,k},\Delta t)$ is the measurement likelihood function.

The measurements are assumed to be independent and identically distributed (i.i.d). The measurement likelihood at the k^{th} CPI in (16) can be factorised by

$$\begin{aligned}
&p(\mathcal{Z}_k,\mathcal{Y}_k|X_k,\alpha_{z,k},\alpha_{y,k},\Delta t)\\
&= l(\mathcal{Z}_k(i_k),\mathcal{Y}_k(j_k)|X_k,\alpha_{z,k},\alpha_{y,k},\Delta t,H=H_1)\prod_{i_k\notin i',j_k\notin j'} l(\mathcal{Z}_k(i'),\mathcal{Y}_k(j')|H=H_0)\\
&= \frac{l(\mathcal{Z}_k(i_k),\mathcal{Y}_k(j_k)|X_k,\alpha_{z,k},\alpha_{y,k},\Delta t,H=H_1)}{l(\mathcal{Z}_k(i_k),\mathcal{Y}_k(i_k)|H=H_0)} l(\mathcal{Z}_k,\mathcal{Y}_k|H=H_0)\\
&\propto L(\mathcal{Z}_k(i_k),\mathcal{Y}_k(j_k)|X_k,\alpha_{z,k},\alpha_{y,k},\Delta t),
\end{aligned} \tag{17}$$

where $l(\cdot|H=H_1)$ is the likelihood under the object existence hypothesis $H=H_1$ and $l(\cdot|H=H_0)$ is the likelihood under the noise only signal hypothesis $H=H_0$. Note that the measurement likelihood in (17) becomes proportional to the instantaneous likelihood ratio $L(\cdot)$ in (14). As a result, the prediction stage in (15) and the update recursion in (16) are rewritten by using the likelihood ratio in (14) i.e.,

$$p(X_k|\mathcal{Z}_{1:k-1}(i_{1:k-1}),\mathcal{Y}_{1:k-1}(j_{1:k-1})) = \int p(X_k|X_{k-1})p(X_{k-1}|\mathcal{Z}_{1:k-1}(i_{1:k-1}),\mathcal{Y}_{1:k-1}(j_{1:k-1}))dX_{k-1} \tag{18}$$

$$p(X_k|\mathcal{Z}_{1:k}(i_{1:k}),\mathcal{Y}_{1:k}(j_{1:k})) \propto L(\mathcal{Z}_k(i_k),\mathcal{Y}_k(j_k)|X_k,\alpha_{z,k},\alpha_{y,k},\Delta t)p(X_k|\mathcal{Z}_{1:k-1}(i_{1:k-1}),\mathcal{Y}_{1:k-1}(j_{1:k-1})), \tag{19}$$

where this filtering computes the posterior density function at the object state X_k in accordance with i_k^{th} range-bearing and doppler bin for the local channel and j_k^{th} range-bearing and doppler bin for the remote channel at the k^{th} CPI.

The Markov transition density is selected as

$$\begin{aligned} p(X_k|X_{k-1}) &= \mathcal{N}(X_k; FX_{k-1}, \Sigma) \\ X_k = FX_{k-1} + b_{k-1}, \quad F &= \begin{bmatrix} 1 & 0 & \Delta & 0 \\ 0 & 1 & 0 & \Delta \\ 0 & 0 & 1 & 0 \\ 0 & 0 & 0 & 1 \end{bmatrix}, \end{aligned} \tag{20}$$

where $X_k = [x_k, y_k, \dot{x}_k, \dot{y}_k]^T$ is the object kinematic parameters, b_{k-1} is the process noise (modelling unknown manoeuvres), which is zero-mean Gaussian with a known covariance Σ, F is the object dynamic matrix, and Δ is the time interval between two consecutive CPIs.

In the proposed algorithm, a sequential Monte Carlo (SMC) realisation of Bayesian recursive filtering known as the particle filter is used [19]. In particular, we use a bootstrap filtering approach for estimating the object trajectory. Given a set of particles $\left\{X_{k-1}^p, \zeta_{k-1}^p\right\}_{p=1}^P$ as the posterior density at $k-1$ state in (19), we obtain P particles $\left\{X_k^p, \zeta_{k-1}^p\right\}_{p=1}^P$ with $X_k^p \sim p(\cdot|X_{k-1}^p)$ sampled from the Markov transition (20) realising the prediction stage in (18).

The posterior density is represented by X_k^p with a weight ζ_k^p. For the update recursion of the object state X_k^p, the corresponding weight ζ_{k-1}^p is updated by the likelihood ratio at the k^{th} CPI in (14), i.e.,

$$\begin{aligned} \zeta_k^p &= \frac{\tilde{\zeta}_k^p}{\sum_{p=1}^P \tilde{\zeta}_k^p}, \\ \tilde{\zeta}_k^p &\propto \zeta_{k-1}^p L(\mathcal{Z}_k(i_k^p), \mathcal{Y}_k(j_k^p)|X_k^p, \alpha_{z,k}^p, \alpha_{y,k}^p, \Delta t), \end{aligned} \tag{21}$$

where ζ_k^p is normalised weight and $\tilde{\zeta}_k^p$ is its un-normalised weight.

After normalising the weights in (21), we test degeneracy of the weighted particles. The degeneracy test is performed by finding the number of effective particles given by

$$N_{eff} = \frac{1}{\sum_{p=1}^P \left(\zeta_k^p\right)^2}, \tag{22}$$

and, testing the degeneracy using N_{eff} compared to a threshold $\mathcal{B}$. When $N_{eff} < \mathcal{B}$, we perform re-sampling (see, e.g., [19]).

Given the set of $\left\{X_k^p, \zeta_k^p\right\}_{p=1}^P$ after the update recursion in (21)–(22), the object state X_k at the k^{th} CPI is estimated by

$$\hat{X}_k = \sum_{p=1}^P \zeta_k^p X_k^p, \tag{23}$$

where $\hat{X}_k$ is the estimated object state X_k. Note that the estimated object state $\hat{X}_k$ in (23) requires estimation of the unknown complex reflection coefficients $\alpha^p_{z,k}$ and $\alpha^p_{y,k}$, which is explained in the next section.

B. Maximum Likelihood estimation of the reflection coefficients

Let us consider estimation of the complex reflection coefficients for evaluating the likelihood ratio in (21). It is assumed that the complex reflection coefficients associated with the local and the remote channels are constant in a CPI, but, these are random variables across consecutive CPIs. We use the maximum likelihood (ML) estimation approach for estimating the reflection coefficients.

Given the object state X^p_k in (21), the corresponding reflection coefficients at the k^{th} CPI are estimated by solving

$$(\hat{\alpha}^p_{z,k}, \hat{\alpha}^p_{y,k}) = \underset{\alpha^p_{z,k}, \alpha^p_{y,k}}{\arg\max} \log \;\; l\big(\mathcal{Z}_k(i^p_k), \mathcal{Y}_k(j^p_k) | X^p_k, \alpha^p_{z,k}, \alpha^p_{y,k}, \Delta t, H = H_1\big), \tag{24}$$

where i^p_k and j^p_k correspond to the bearing-range and doppler bins associated with $(\theta^p_k, r^p_k, \omega^p_{d_k})$ of X^p_k, $\log l(\cdot|H = H_1)$ is the natural logarithm of the likelihood under the object existence hypothesis in (12), and, $\hat{\alpha}^p_{z,k}$ and $\hat{\alpha}^p_{y,k}$ denote the ML estimate of $\alpha^p_{z,k}$ and $\alpha^p_{y,k}$.

For solving (24), after taking the natural logarithm of the likelihood in (12), we obtain

$$\begin{aligned}
&\log l\big(\mathcal{Z}_k(i^p_k), \mathcal{Y}_k(j^p_k) | X^p_k, \alpha^p_{z,k}, \alpha^p_{y,k}, \Delta t, H = H_1\big) = -2LN \log(\pi) \\
&- \log\big(\det(\Sigma_z)\big) - \log\big(\det(\Sigma_y)\big) - \mathcal{Z}_k(i^p_k)^H \Sigma_z^{-1} \mathcal{Z}_k(i^p_k) - \mathcal{Y}_k(j^p_k)^H \Sigma_y^{-1} \mathcal{Y}_k(j^p_k) \\
&+ 2\,\mathrm{Re}\Big(\alpha^{*p}_{z,k} s_{z,k}(X^p_k)^H \Sigma_z^{-1} \mathcal{Z}_k(i^p_k)\Big) + 2\,\mathrm{Re}\Big(\alpha^{*p}_{y,k} s_{y,k}(\Delta t)^H \Sigma_y^{-1} \mathcal{Y}_k(j^p_k)\Big) \\
&- |\alpha^p_{z,k}|^2 s_{z,k}(X^p_k)^H \Sigma_z^{-1} s_{z,k}(X^p_k) - |\alpha^p_{y,k}|^2 s_{y,k}(\Delta t)^H \Sigma_y^{-1} s_{y,k}(\Delta t),
\end{aligned} \tag{25}$$

where * denotes the complex conjugate transpose, $(\cdot)^H$ represents the Hermitian transpose of its input argument, and $\mathrm{Re}(\cdot)$ takes the real part of its complex argument.

Afterwards, we take the partial derivative of (25) with respect to $\alpha^p_{z,k}$ for the local channel and $\alpha^p_{y,k}$ for the remote channel, and, obtain

$$\begin{aligned}
&\frac{\partial \log l\big(\mathcal{Z}_k(i^p_k), \mathcal{Y}_k(j^p_k) | X^p_k, \alpha^p_{z,k}, \alpha^p_{y,k}, \Delta t, H = H_1\big)}{\partial \alpha^p_{z,k}} = \\
&2 s_{z,k}(X^p_k)^H \Sigma_z^{-1} \mathcal{Z}_k(i^p_k) - 2\alpha^p_{z,k} s_{z,k}(X^p_k)^H \Sigma_z^{-1} s_{z,k}(X^p_k), \quad \text{and,} \\
&\frac{\partial \log l\big(\mathcal{Z}_k(i^p_k), \mathcal{Y}_k(j^p_k) | X^p_k, \alpha^p_{z,k}, \alpha^p_{y,k}, \Delta t, H = H_1\big)}{\partial \alpha^p_{y,k}} = \\
&2 s_{y,k}(\Delta t)^H \Sigma_y^{-1} \mathcal{Y}_k(j^p_k) - 2\alpha^p_{y,k} s_{y,k}(\Delta t)^H \Sigma_y^{-1} s_{y,k}(\Delta t).
\end{aligned} \tag{26}$$

The ML solution in (24) is found by setting (26) to zero, i.e.,

$$\hat{\alpha}^p_{z,k} = \frac{s_{z,k}(X^p_k)^H \Sigma_z^{-1} \mathcal{Z}_k(i^p_k)}{s_{z,k}(X^p_k)^H \Sigma_z^{-1} s_{z,k}(X^p_k)}, \tag{27}$$

$$\hat{\alpha}^p_{y,k} = \frac{s_{y,k}(\Delta t)^H \Sigma_y^{-1} \mathcal{Y}_k(j^p_k)}{s_{y,k}(\Delta t)^H \Sigma_y^{-1} s_{y,k}(\Delta t)}, \tag{28}$$

where $s_{z,k}(\cdot) \in \mathbb{C}^{LN\times 1}$ is the noise free signal model given X^p_k in (6), $s_{y,k}(\Delta t) \in \mathbb{C}^{LN\times 1}$ is the noise free signal model associated with the unknown synchronisation term Δt in (9), $\hat{\alpha}^p_{z,k}$ is the ML estimate of $\alpha^p_{z,k}$ associated with the local channel, and $\hat{\alpha}^p_{y,k}$ represents the ML estimate of $\alpha^p_{y,k}$ associated with the remote channel. Note that $\alpha^p_{y,k}$ in (28) requires estimation of the synchronisation term Δt. We use two synchronisation approaches for estimating Δt which are explained in Section IV.

IV. Synchronisation of the detector with the remote transmitters

A. Synchronisation term estimation for the bi-static only case

The first approach we consider for estimation of Δt is to use the bi-static setting and we name the bi-static synchronisation approach. This approach utilises a digital beam-forming with the ULA structure to simultaneously divert beams to collect both the reflected signals in the remote channel and the direct signals in the direct channel when the omni-directional transmitter is used. Therefore, the received signals in the remote channel contain a unknown time shift Δt equivalent to Δt received in the direct channel. Let us consider the data vector in the direct channel using (7), i.e.,

$$\mathbf{D}(l) = \sqrt{E} s_d(l_1\Delta\theta, l_2\Delta r + \Delta t) + n_d(l_1\Delta\theta, l_2\Delta r), \tag{29}$$

where $l_k = [l_1, l_2]$ corresponds to the bearing-range bin associated with the location (θ_t, r_t) of the separated transmitter, E is the known energy of the signal at the receiver front-end, and n_d is a complex Gaussian noise variable with zero mean and covariance Σ_d.

Now, we use a time shifted version of the direct channel for evaluating the sufficient statistics. An amount of time shifting the measurement $\mathbf{D}(l)$ in (29) is specified by the location of the separated transmitter. This version at the k^{th} CPI is found as

$$\begin{aligned} \mathcal{D}_k(l) &= \mathbf{D}_k(l) \odot s_d(-\theta_t, -r_t) \\ &= \sqrt{E} s_d(0, \Delta t) + n_{d,k}(l_1, l_2) \\ &= \sqrt{E} s_d(\Delta t) + n_{d,k}(l_1, l_2), \end{aligned} \tag{30}$$

where $\mathcal{D}_k(\cdot)$ is the shifted version of the measurement in the direct channel.

In order to find Δt, we estimate $s_d(\Delta t)$ instead of Δt, and, use the ML estimation approach with the measurements from $n = 1$ to k in (30), i.e.,

$$\hat{s}_d(\Delta t) = \underset{s_d(\Delta t)}{\arg\max} \log \; l(\mathcal{D}_{1:k}(l)|s_d(\Delta t)), \tag{31}$$

where $l(\mathcal{D}_{1:k}(l)|s_d(\Delta t))$ is the measurement likelihood in the direct channel given by

$$\begin{aligned} l(\mathcal{D}_{1:k}(l)|s_d(\Delta t)) &= \left(\frac{1}{\pi^{LN}\det(\Sigma_d)}\right)^k \times \\ &\exp\left(\sum_{n=1}^{k} -(\mathcal{D}_n(l) - \sqrt{E}s_d(\Delta t))^H \Sigma_d^{-1} (\mathcal{D}_n(l) - \sqrt{E}s_d(\Delta t))\right). \end{aligned} \tag{32}$$

After taking partial derivative of $\log$ likelihood in (32) with respect to the $s_d(\Delta t)$, and, setting to zero, the ML solution for the $s_d(\Delta t)$ is found as

$$\hat{s}_d(\Delta t) = \frac{1}{k}\sum_{n=1}^{k} \frac{\mathcal{D}_n(l)}{\sqrt{E}}, \tag{33}$$

where the synchronisation term Δt in $\hat{s}_d(\Delta t)$ is equivalent to Δt in the remote channel, and, we substitute $\hat{s}_d(\Delta t)$ in (28) so as to estimate the complex reflection coefficient associated with the remote channel.

B. Synchronisation term estimation for the multi-static case

Next, we consider estimation of Δt using the multi-static setting, which is named as the multi-static synchronisation approach. This approach uses the object trajectory estimated with the local channel to find Δt in the remote channel. This also enables us to remove the constraint on the omni-directionality of the transmitter so that the receiver collects the direct signals emitted by the separated transmitter described in Section IV-A.

Given the set of $\left\{X_k^p\right\}_{p=1}^P$ after the prediction stage in (18), we can define a marginal likelihood, i.e.,

$$\begin{aligned} l_M\big(\mathcal{Z}_k(i_k), \mathcal{Y}_k(j_k)|\Delta t\big) &= \int l\big(\mathcal{Z}_k(i_k), \mathcal{Y}_k(j_k)|X_k, \hat{\alpha}_{z,k}, \hat{\alpha}_{y,k}, \Delta t\big) \\ &\quad \times p\big(X_k|\mathcal{Z}_{1:k-1}(i_{1:k-1}), \mathcal{Y}_{1:k-1}(j_{1:k-1})\big) dX_k \\ &\approx \sum_{p=1}^{P} l\big(\mathcal{Z}_k(i_k^p), \mathcal{Y}_k(j_k^p)|X_k^p, \hat{\alpha}_{z,k}^p, \hat{\alpha}_{y,k}^p, \Delta t\big), \end{aligned} \tag{34}$$

where $l_M\big(\mathcal{Z}_k(i_k), \mathcal{Y}_k(i_k)|\Delta t\big)$ is the marginal likelihood function, and, $\hat{\alpha}^p_{z,k})$ and $\hat{\alpha}^p_{y,k}$ are the ML estimate of the complex reflection coefficients given in (27) and (28), respectively.

The marginal likelihood in (34) can be factorised as

$$\begin{aligned} l_M\big(\mathcal{Z}_k(i_k), \mathcal{Y}_k(j_k)|\Delta t\big) &\approx \sum_{p=1}^{P} l\big(\mathcal{Z}_k(i^p_k)|X^p_k, \hat{\alpha}^p_{z,k}\big) l\big(\mathcal{Y}_k(j^p_k)|X^p_k, \hat{\alpha}^p_{y,k}, \Delta t\big) \\ &\propto \sum_{p=1}^{P} l\big(\mathcal{Y}_k(j^p_k)|X^p_k, \hat{\alpha}^p_{y,k}, \Delta t\big) \\ &\propto \sum_{p=1}^{P} \frac{1}{\pi^{LN}\det(\Sigma_y)} \exp\Big(-\mathcal{Y}_k(j^p_k)^H \Sigma_y^{-1} \mathcal{Y}_k(j^p_k)\Big) \exp\Big(\frac{|s_{y,k}(\Delta t)^H \Sigma_y^{-1} \mathcal{Y}_k(i^p_k)|^2}{s_{y,k}(\Delta t)^H \Sigma_y^{-1} s_{y,k}(\Delta t)}\Big) \\ &\propto \sum_{p=1}^{P} \exp\Big(\frac{|s_{y,k}(\Delta t)^H \Sigma_y^{-1} \mathcal{Y}_k(i^p_k)|^2}{s_{y,k}(\Delta t)^H \Sigma_y^{-1} s_{y,k}(\Delta t)}\Big), \end{aligned} \tag{35}$$

Here, the marginal likelihood $l_M(.)$ in (35) only contains the synchronisation term Δt.

For estimating Δt, we use the ML estimator using the natural logarithm of the marginal likelihood in (35). We also apply a window so that the estimation of Δt is considered with measurements from $k-w$ to k where k indicates the k^{th} CPI and w is the window length. Thus, Δt is determined by solving

$$\begin{aligned} \hat{\Delta t} &= \arg\max_{\Delta t} \ \log \prod_{m=k-w}^{k} l_M\big(\mathcal{Z}_m(i_m), \mathcal{Y}_m(i_m)|\Delta t\big) \\ &= \arg\max_{\Delta t} \sum_{m=k-w}^{k} \sum_{p=1}^{P} \Big(\frac{|s_{y,m}(\Delta t)^H \Sigma_y^{-1} \mathcal{Y}_m(i^p_m)|^2}{s_{y,m}(\Delta t)^H \Sigma_y^{-1} s_{y,m}(\Delta t)}\Big) \end{aligned} \tag{36}$$

where $\Delta \hat{t}$ is the ML estimate of Δt.

In order to find the maximum value of Δt in (36), we use a golden section search algorithm in one dimension with the range of $[\Delta t_{min}, \Delta t_{max}]$ (see, e.g., [20, Chp.10]). This algorithm is described in Algorithm 1.

V. Long time integration for detection

A. Long time integration

In this section, we consider long time integration based on the estimated parameters so as to decide on the object existence hypothesis. In order to perform this proposed integration, we first estimate $\hat{X}_k$ by using SMC recursion and (23). We then substitute $\hat{X}_k$ and $\Delta \hat{t}$ in (27) and (28) in order to estimate $\hat{\alpha}_{z,k}$ and $\hat{\alpha}_{y,k}$, respectively.

Algorithm 1 Maximum likelihood estimation of Δt via golden section search

1: Initialisation: Set

$$a = \Delta t_{min}, \quad b = \Delta t_{max}$$

$$g = \frac{\sqrt{5}-1}{2}, \quad \text{and} \quad f(\Delta t) = \sum_{m=k-w}^{k} \sum_{p=1}^{P} \Big(\frac{|s_{y,m}(\Delta t)^H \Sigma_y^{-1} \mathcal{Y}_m(j_m^p)|^2}{s_{y,m}(\Delta t)^H \Sigma_y^{-1} s_{y,m}(\Delta t)} \Big)$$

2: Find the boundaries of Δt using $x_1 = a + (b-a) \times (1-g)$ and $x_2 = a + (b-a) \times g$
3: Compute $f(x_1)$ and $f(x_2)$
4: **while** $|x_1 - x_2| > A_c$(i.e., accuracy of estimation) **do**
5: **if** $f(x_1) > f(x_2)$ **then**
6: Set new boudaries $b = x_2$ and $x_2 = x_1$
7: Find $x_1 = a + (b-a) \times (1-g)$
8: Compute $f(x_1)$ and $f(x_2)$
9: **else**
10: Set new boudaries $a = x_1$ and $x_1 = x_2$
11: Find $x_2 = a + (b-a) \times (g)$
12: Compute $f(x_1)$ and $f(x_2)$
13: **end if**
14: **end while**
15: **if** $f(x_1) > f(x_2)$ **then**
16: Estimate $\Delta \hat{t} = x_1$
17: **else**
18: Estimate $\Delta \hat{t} = x_2$
19: **end if**

Afterwards, we substitute $\hat{X}_k$, $\hat{\alpha}_{z,k}$, $\hat{\alpha}_{y,k}$, and $\Delta \hat{t}$ in the natural logarithm of the likelihood ratio in (11) for $k = 1, \cdots, K$. As a result, the detection is performed by

$$\begin{aligned} &\log L\big(\mathcal{Z}_{1:K}(\hat{i}_{1:K}), \mathcal{Y}_{1:K}(\hat{j}_{1:K}) | \hat{X}_{1:K}, \hat{\alpha}_{z,1:K}, \hat{\alpha}_{y,1:K}, \Delta \hat{t}\big) \\ &= \sum_{k=1}^{K} \left(\frac{|s_{z,k}(\hat{X}_k)^H \Sigma_z^{-1} \mathcal{Z}_k(\hat{i}_k)|^2}{s_{z,k}(\hat{X}_k)^H \Sigma_z^{-1} s_{z,k}(\hat{X}_k)} + \frac{|s_{y,k}(\Delta \hat{t})^H \Sigma_y^{-1} \mathcal{Y}_k(\hat{j}_k)|^2}{s_{y,k}(\Delta \hat{t})^H \Sigma_y^{-1} s_{y,k}(\Delta \hat{t})} \right) \underset{H_0}{\overset{H_1}{\gtrless}} \log \mathcal{T}_K, \end{aligned} \tag{37}$$

where $\log \mathcal{T}_K$ is the detection threshold for a given constant false alarm rate (CFAR) for K steps of integration.

Algorithm 2 The proposed simultaneous tracking and long time integration algorithm

Initialisation: generate a set of particles $\left\{X_0^p, \zeta_0^p\right\}_{p=1}^P$
for k = 1 to K (processing of K CPIs) **do**
    Collect measurements and store in $\mathcal{Z}_k$ and $\mathcal{Y}_k$ given in (10)
    for p = 1 to P (processing of SMC with P particles) **do**
        Prediction: draw particle $X_k^p \sim p(X_k^p|X_{k-1}^p)$ using (20)
    end for
    Estiamte Δt using (33) when the direct channel is available
    Estiamte Δt using (36) when the direct channel is not available
    for p = 1 to P (processing of SMC with P particles) **do**
        Update: compute $\tilde{\zeta}_k^p$ using substition of $\hat{\alpha}_{z,k}^p$, $\hat{\alpha}_{y,k}^p$ and $\Delta\hat{t}$ in (21)
    end for
    Normalise $\tilde{\zeta}_k^p$
    Degeneracy test in (22)
    Estimate $\hat{X}_k$ using (23)
    Estimate $\hat{\alpha}_{z,k}$ and $\hat{\alpha}_{y,k}$ using substitution $\hat{X}_k$ and $\Delta\hat{t}$ in (27) and (28)
    Perform detection test using the proposed long time integration in (37)
end for

Note that the proposed integration approach in (37) performs coherent integration of $L \times N$ samples in a CPI at each channel and non-coherent integration across these channels as well as consecutive CPIs, while taking into account the object trajectory. The overall process of the proposed detection algorithm is described in Algorithm 2.

B. Constant false alarm rate threshold for detection test

Let us consider the detection threshold $\mathcal{T}_K$ in (37) for a constant false alarm rate (CFAR). This threshold can be calculated by using a function of a selected probability of false alarm rate P_{fa}. For this purpose, we define a likelihood under the noise only signal hypothesis across channels. This likelihood can be evaluated by the sum of the local and the remote channels for

K steps of integration using (10) for $\Sigma_z = \sigma_z^2\mathbf{I}$ and $\Sigma_y = \sigma_y^2\mathbf{I}$, i.e.,

$$\begin{aligned} &p(Z_K|H = H_0) = \mathcal{CN}(.; 0, KLN(\sigma_z^2 + \sigma_y^2)), \\ &\mathbb{E}\{Z_K\} = \mathbb{E}\{\mathcal{Z}_K + \mathcal{Y}_K\} = \mathbb{E}\{\mathcal{Z}_K\} + \mathbb{E}\{\mathcal{Y}_K\} = 0 \\ &\mathbb{E}\{Z_K^2\} = \mathbb{E}\{(\mathcal{Z}_K + \mathcal{Y}_K)^2\} = \mathbb{E}\{\mathcal{Z}_K^2\} + 2\mathbb{E}\{\mathcal{Z}_K\}\mathbb{E}\{\mathcal{Y}_K\} + \mathbb{E}\{\mathcal{Y}_K^2\} \\ &= KLN\sigma_z^2 + KLN\sigma_y^2, \end{aligned} \tag{38}$$

where $\mathbb{E}\{Z_K\}$ is the mean value, $\mathbb{E}\{Z_K^2\}$ is the variance, and $\mathbb{E}\{\cdot\}$ denotes the expectation of its input argument. Hence, the likelihood $p(Z_k|H = H_0)$ can be defined as

$$p(Z_K|H_0) = \frac{1}{\pi KLN(\sigma_z^2 + \sigma_y^2)} \exp\left(-\frac{|Z_K|^2}{KLN(\sigma_z^2 + \sigma_y^2)}\right). \tag{39}$$

Next, we find the P_{fa} for the detection test by integrating $p(Z_K|H = H_0)$ when Z_K is over the detection threshold $\mathcal{T}_K$. The P_{fa} can be defined as

$$\begin{aligned} &P_{fa} = \int_{\mathcal{T}_K}^{+\infty} p(Z_K|H = H_0)dZ_K = \frac{1}{\pi\sqrt{KLN(\sigma_z^2 + \sigma_y^2)}} \times \\ &\int_{\frac{\mathcal{T}_K}{\sqrt{KLN(\sigma_z^2+\sigma_y^2)}}}^{+\infty} \exp\left(-|t|^2\right) dt = \frac{1}{2\sqrt{\pi KLN(\sigma_z^2 + \sigma_y^2)}} \mathrm{erfc}\left(\frac{\mathcal{T}_K}{\sqrt{KLN(\sigma_z^2 + \sigma_y^2)}}\right), \end{aligned} \tag{40}$$

where $\mathrm{erfc}(.)$ denotes the complementary error function (see, e.g, [3, Chp.6]). As a result, the threshold $\mathcal{T}_K$ given P_{fa} for K steps of integration using (40) is found as

$$\mathcal{T}_K = \sqrt{KLN(\sigma_z^2 + \sigma_y^2)}\mathrm{erfc}^{-1}\left(2\sqrt{\pi KLN(\sigma_z^2 + \sigma_y^2)}P_{fa}\right), \tag{41}$$

where $\mathrm{erfc}^{-1}(.)$ is the inverse complementary error function. Given a probability of false alarm rate P_{fa}, we can calculate $\mathcal{T}_K$ using (41) for the likelihood ratio test in (37) for K steps of integration.

VI. Example

In this section, we demonstrate the proposed algorithm through an example and compare the efficacy of this approach with conventional techniques. We consider a scenario in which a ULA receiver co-located with a transmitter is at the origin of the 2D Cartesian plane, and, a separated transmitter is located at $[10\mathrm{m}, 500\mathrm{m}]$ (see. Fig. 2). In this setting, two transmitters emit $N = 20$ linear frequency modulated (i.e., chirp) waveforms in a CPI towards a surveillance region. In this region, there is a low SNR object with an initial state $X_0 = [1000\mathrm{m}, 1000\mathrm{m}, 10\mathrm{m/s}, 50\mathrm{m/s}]$

TABLE I: Transmitted signal parameters

Parameter	Value
Carrier frequency f_c	10GHz
Bandwidth B	1MHz
Pulse repetition interval (PRI) T	100us
Coherent processing interval (CPI) Δ	0.1s
Number of pulses during a CPI N	20
Number of elements in ULA L	20
Number of transmitters M	2

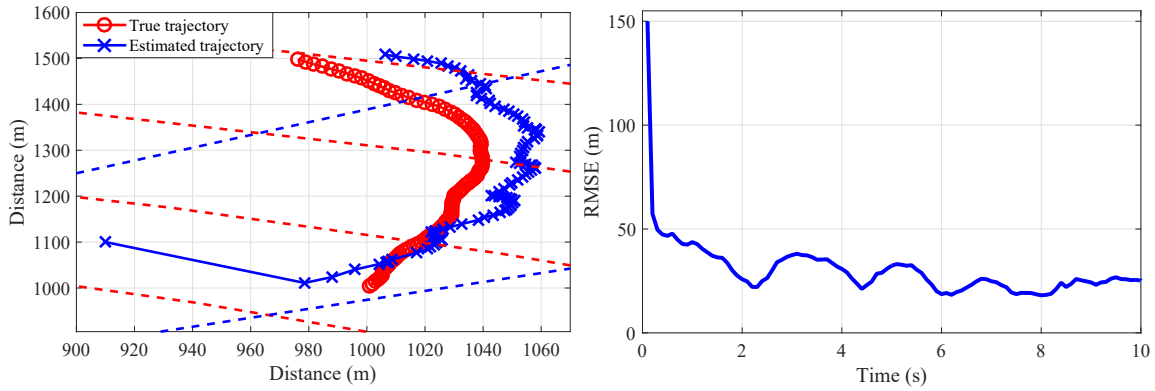

(a) Typical scenario for an estimated trajectory

(b) Root mean square error (RMSE)

Fig. 3: Example scenario: (a) A low SNR (-6dB) object moves the true trajectory (red line) across range (red dashed lines) and bearing (blue dashed lines) bins. The proposed algorithm estimates the object trajectory (blue line) for detection test. (b) RMSE (blue line) of this trajectory estimate obtained in (a).

moving along an unknown trajectory according to the object dynamic model described in (20). The ULA receiver collects measurements in accordance with the signal model in (10) in both the local and the remote channels as well as the direct channel.

The parameters of the transmitted pulses used in this example are shown in Table I. Given these parameters, we calculate the bearing resolution as $\Delta\theta = 5.1^\circ$ given by $\Delta\theta = \sin^{-1}\left(\frac{0.8192}{L}\right)$, and, the range resolution as $\Delta r = 150$m given by $\Delta r = \frac{c}{2B}$ (see, e.g., [15]). Fig 3 illustrates these corresponding resolutions, where the blue dashed lines and the red dashed lines indicate the bearing resolutions and the range resolutions, respectively. The velocity resolution as $\Delta V =$

$7.5\mathrm{m/s}$ is also found by using $\Delta V = \frac{\lambda_c}{2NT}$ (or, equivalently, the doppler resolution $\Delta\omega = 4\pi f_c \frac{\Delta V}{c} T$ as $0.314\mathrm{deg/s}$).

We use the proposed algorithm to test the object existence hypothesis in the receiver's resolution bins with $P = 400$ particles. These particles are initially selected as a 20×20 element uniform grid within the bin under test. We perform long time integration using (37) spanning $10\mathrm{s}$ with a CPI interval of $0.1\mathrm{s}$. The complex reflection coefficient for each channel is also generated using a complex Gaussian density leading to an expected SNR of $-6\mathrm{dB}$. For synchronisation, we deal with the synchronisation term Δt in the remote channel as an unknown time shift and randomly select Δt in the range of $0 < \Delta t < PRI$ so that each received pulse in the remote channel contains the unknown time shift. We also generate the direct signals with additive noise using (29) leading to an expected SNR of $0\mathrm{dB}$.

In this example, when an object is located in the bin under test, the particles generated by the proposed algorithm converge to the underlying state of the object, and, the integrated value using the proposed integration in (37) increases. When this value is over the detection threshold, the proposed algorithm selects the object existence hypothesis. On the other hand, when the bin under test contains no object, the particles start to diverge in space due to very small and similar likelihood values. Fig. 3(a) illustrates a typical trajectory estimate using the proposed algorithm, which indicates that the trajectory estimate (blue line) is reasonably close to the true trajectory (red line). Fig. 3(b) shows the root mean square error (RMSE) of this trajectory estimate (blue line) obtained in Fig. 3(a), where the RMSE provides a reasonably low value after only a few steps (i.e., each step represents a CPI).

Now, we consider long time integration. For this purpose, we generate 100 measurement sets using (10) with unknown object trajectories described in Fig 3 and perform long time integration using two synchronisation approaches described in Section IV. We then evaluate the detection performance based on these two approaches.

A. Long time integration using the bi-static synchronisation approach

First, we consider long time integration obtained by using the bi-static synchronisation approach explained in Section IV-A. Fig. 4(a) illustrates the average integrated value (blue solid line) with ± 1 standard deviation bounds (blue dotted line) using the proposed approach. It can be seen that the integrated value using the proposed integration increases up to 42.7 at $t = 10\mathrm{s}$, which is relatively close to the best achievable value (red dashed line) 51.78 using

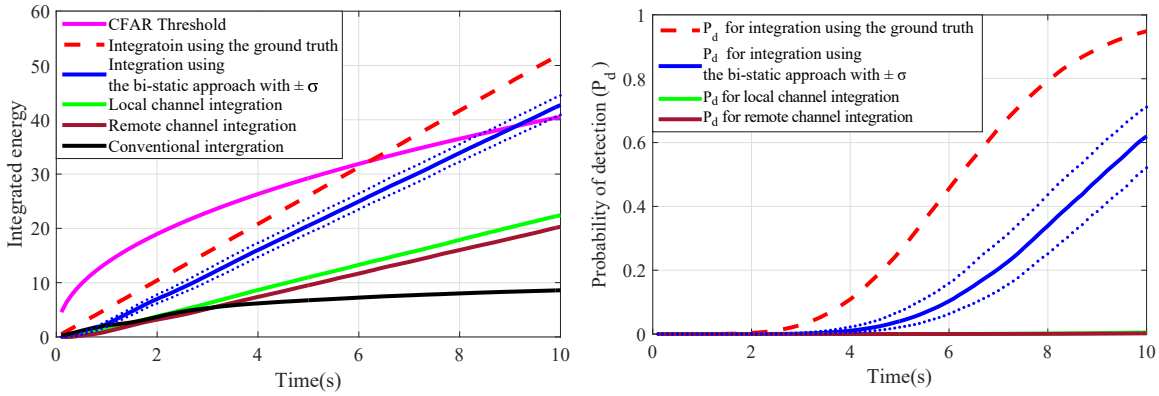

(a) Long-time integration

(b) Probability of detection

Fig. 4: Long-time integration obtained by using the bi-static synchronisation approach: (a) The average proposed integration (blue line) using the proposed algorithm versus the integration with ground truth (red dashed line) compared to the detection (CFAR) threshold (magenta line). The conventional coherent (black line), the local channel (green line), and the remote channel (brown line) integration fail to exceed the detection threshold. (b) The corresponding probabilities of detection (P_d) with the same colour code found in (a).

the full knowledge of the ground truth values of the trajectory and the synchronisation term of the remote channel. Here, we calculate the detection threshold as the CFAR threshold (magenta line) using (41) for the given probability of false alarm rate $P_{fa} = 10^{-8}$ and compare the integrated values against this threshold. It is clearly observed that the integrated value using the proposed approach exceeds the CFAR threshold at $t = 9.1$s, while both the local channel (green solid line) and the remote channel (brown solid line) integration stay under the noise only signal hypothesis. The conventional coherent integration (black solid line) also selects the noise only signal hypothesis. Note that when the integration is used with an individual channel, this integrated value fails to exceed the detection threshold due to the inferior tracking performance.

Now, we consider the probability of detection P_d as the function of the integrated value over time, and, calculate this probability for the proposed algorithm empirically. Fig. 4(b) illustrates the P_d (blue solid line) with ± 1 standard deviation bounds (blue dotted lines) for the proposed integration compared to the P_d (red dashed line) obtained by the best achievable integration. It clearly appears that the P_d using the proposed integration increases over time and reaches 0.62 at $t = 10$s, whereas both P_ds for the local (green solid line) and the remote integration (brown solid line) reach almost zero and fail to detect the object in an overwhelming majority of the

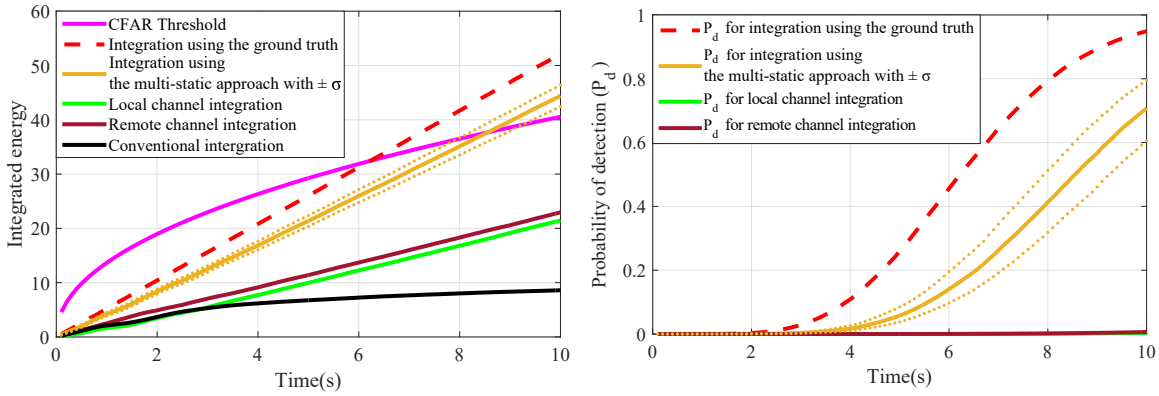

(a) Long-time integration

(b) Probability of detection

Fig. 5: Long-time integration using the multi-static synchronisation approach: (a) The average integration value (orange line) using the multi-static synchronisation approach versus the integration with ground truth (red dashed line) compared to the detection (CFAR) threshold (magenta line). The conventional coherent (black line), and the local channel (green line), and the remote channel (brown line) integration fail to exceed the CFAR threshold. (b) The corresponding probabilities of detection (P_d) with the same colour code found in (a).

experiences.

B. Long time integration using the multi-static synchronisation approach

In the second case, we consider long time integration obtained by using the multi-static synchronisation approach in (36) with the window length $w = 5$ explained in Section IV-B. Fig 5(a) illustrates the average integrated value (orange solid line) with ± 1 standard deviation bounds (orange dotted line) using the proposed algorithm in comparison with the best achievable values (red dashed line) obtained by using the full knowledge of the ground truth information described in Fig. 4(a). It can be seen that the proposed integrated value (orange solid line) reaches up to 44.41 at $t = 10$s, which is reasonably close to the best achievable integration value 51.78. Next, we compare the integrated values to the same CFAR threshold (magenta line) in Fig. 4(a). It is recognised that the proposed integrated value exceeds the CFAR threshold at $t = 8.4$s, while both integrated values in the local channel (green line) and the remote channel (brown line) select the noise only signal hypothesis. The integrated value using the conventional coherent integration also decides on the noise only signal hypothesis.

For the probability of detection, Fig. 5(b) illustrates the P_d for the proposed integration (orange

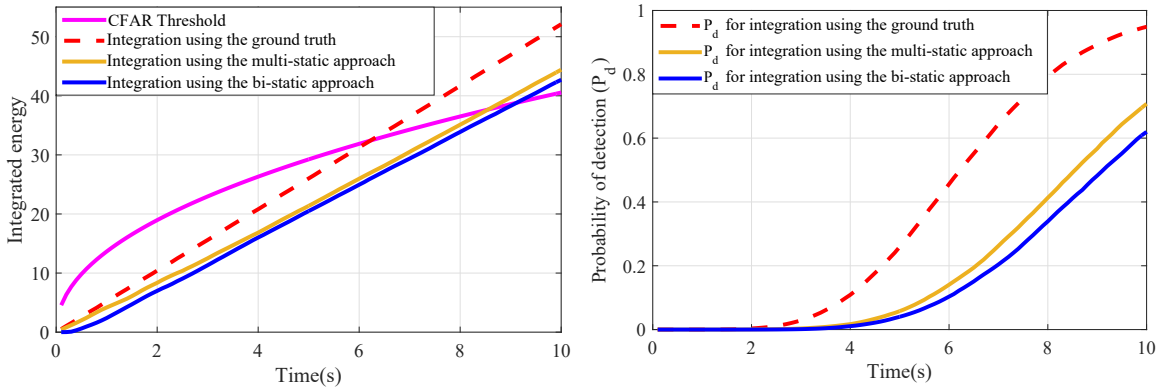

(a) Long-time integration

(b) Probability of detection

Fig. 6: Comparison between the bi-static synchronisation approach and the multi-static synchronisation approach: (a) The average long time integration (orange solid line) using the multi-static synchronisation approach versus the average integration (blue solid line) using the bi-static synchronisation approach. (b) The corresponding P_ds of these integrated values found in (a).

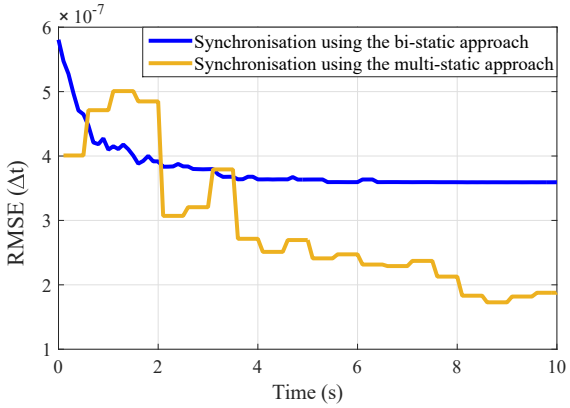

Fig. 7: RMSE of the synchronised term estimated by using the bi-static synchronisation approach (blue solid line) and using the multi-static synchronisation approach (orange solid line)

solid line) with ± 1 standard deviation bounds (orange dotted line). It is clearly observed that the P_d using the proposed integration reaches up to 0.70 at $t = 10$s, whereas both P_ds for the local and the remote channel integration reach almost zero and fail to detect the object.

C. Comparison

Let us compare the two aforementioned approaches. Fig 6(a) shows the average long time integration (orange solid line) obtained by using the multi-static synchronisation approach and the average long time integration (blue solid line) obtained by using the bi-static synchronisation approach. It can be seen that the integrated value using the multi-static synchronisation

approach reaches higher value 44.41 at $t = 10$s than the integrated value 42.7 using the bi-static synchronisation approach. When the integrated values are compared to the detection threshold, the integrated value (orange solid line) exceeds the CFAR threshold (magenta line) at $t = 8.4$s, which is faster than the integrated value (blue solid line) at $t = 9.1$s. Fig 6(b) also illustrates the corresponding probabilities of detection P_ds using the same colour code in Fig 6(a). It is clearly observed that the P_d for the integration (orange solid line) using the multi-static synchronisation approach reaches 0.70 at $t = 10$s higher than the P_d (blue solid line) using the bi-static synchronisation approach as 0.62.

Next, we compare these two approaches based on estimation of the synchronisation term Δt. For this purpose, we calculate the RMSE of the estimated Δt given by

$$RMSE(\Delta t) = \sqrt{\frac{\sum_m^M (\Delta \hat{t}_{m,k} - \Delta t)}{M}} \tag{42}$$

where Δt indicates the true synchronisation term, $\Delta \hat{t}_{m,t}$ is the m^{th} estimate of Δt at the k^{th} CPI and $M = 100$ is the total measurement sets.

Fig 7 illustrates the RMSEs of Δt estimated by using these two approaches. It is clearly recognised that the RMSE of Δt using the multi-static synchronisation approach (orange line) is much lower than when using the bi-static synchronisation approach (blue line).

The benefits of these approaches come with some additive cost of computations compared to conventional integration methods. The computational cost of the bin under test for detection using the proposed algorithm at the k^{th} CPI requires $P(N_X^2 + 2M(LN)^2)$ multiplications and $P(1 + 2M(LN - 1))$ additions for using the bi-static synchronisation approach, and, $P(N_X^2 + 2N_I M(LN)^2)$ multiplications and $P(1 + 2N_I M(LN - 1))$ additions for using the multi-static synchronisation approach, while conventional coherent integration requires M multiplications and $M(LN - 1)$ additions. Here, N_X denotes the dimensionality of the object state in (20) and N_I is the number of iterations for the golden selection search in Algorithm 1.

VII. Conclusion

In this work, we have proposed a detection approach, which can perform simultaneous trajectory estimation and log time integration for detecting a manoeuvring and low SNR object in mono-static, bi-static, and multi-static configurations. We demonstrate that this proposed algorithm provides long time integration, which performs coherent integration of reflections within a CPI in all these configurations together with non-coherent integration across the channels

as well as consecutive CPSs. It is found that the proposed integrated value is close to the best achievable integrated value using the ground truth values of the true trajectory and the synchronisation term of the remote channel. For synchronisation, we present the bi-static and the multi-static synchronisation approaches. The benefit of the multi-static synchronisation approach enables us to remove the need for the omni-directionality of the transmitter when the bi-static synchronisation approach is used. It is also found that the multi-static synchronisation approach provides lower error value of estimating the synchronisation term than when using the bi-static synchronisation approach. Future work includes further experimentation for the characterisation of this detection approach under different SNR working conditions.

REFERENCES

[1] M. Richards, W. Melvin, J. Scheer, J. Scheer, and W. Holm, *Principles of Modern Radar: Radar Applications*, ser. Electromagnetics and Radar. Institution of Engineering and Technology, 2014. [Online]. Available: https://books.google.co.uk/books?id=tYfYAgAAQBAJ

[2] S. Haykin, "Cognitive radar: a way of the future," *IEEE Signal Processing Magazine*, vol. 23, no. 1, pp. 30–40, Jan 2006.

[3] M. Richards, *Fundamentals of Radar Signal Processing*, ser. Professional Engineering. Mcgraw-hill, 2005. [Online]. Available: https://books.google.co.uk/books?id=VOvsJ7G1oDEC

[4] X. Chen, J. Guan, N. Liu, and Y. He, "Maneuvering target detection via radon-fractional fourier transform-based long-time coherent integration," *Signal Processing, IEEE Transactions on*, vol. 62, no. 4, pp. 939–953, Feb 2014.

[5] Y. Boers and J. Driessen, "Multitarget particle filter track before detect application," *Radar, Sonar and Navigation, IEE Proceedings*, vol. 151, no. 6, pp. 351–357, Dec 2004.

[6] E. Grossi, M. Lops, and L. Venturino, "A novel dynamic programming algorithm for track-before-detect in radar systems," *Signal Processing, IEEE Transactions on*, vol. 61, no. 10, pp. 2608–2619, May 2013.

[7] H. L. Van Trees, *Detection, Estimation, and Modulation Theory: Radar-Sonar Signal Processing and Gaussian Signals in Noise*. Melbourne, FL, USA: Krieger Publishing Co., Inc., 1992. [Online]. Available: http://portal.acm.org/citation.cfm?id=530789

[8] S. Davey, M. Rutten, and B. Cheung, "Using phase to improve track-before-detect," *Aerospace and Electronic Systems, IEEE Transactions on*, vol. 48, no. 1, pp. 832–849, Jan 2012.

[9] M. Uney, B. Mulgrew, and D. Clark, "Maximum likelihood signal parameter estimation via track before detect," pp. 1–5, Sept 2015.

[10] O. Rabaste, C. Riche, and A. Lepoutre, "Long-time coherent integration for low snr target via particle filter in track-before-detect," in *Information Fusion (FUSION), 2012 15th International Conference on*, July 2012, pp. 127–134.

[11] K. Kim, M. Uney, and B. Mulgrew, "Detection of manoeuvring low snr objects in receiver arrays," in *2016 Sensor Signal Processing for Defence (SSPD)*, Sept 2016, pp. 1–5.

[12] ——, "Simultaneous tracking and long time integation for detection in collaborative array radars," in *2017 IEEE Radar Conference (RadarConf17), to appear*, May 2017, pp. 1–6.

[13] H. Godrich, A. Haimovich, and R. Blum, "Target localization accuracy gain in mimo radar-based systems," *Information Theory, IEEE Transactions on*, vol. 56, no. 6, pp. 2783–2803, June 2010.

[14] R. Niu, R. Blum, P. Varshney, and A. Drozd, "Target localization and tracking in noncoherent multiple-input multiple-output radar systems," *Aerospace and Electronic Systems, IEEE Transactions on*, vol. 48, no. 2, pp. 1466–1489, April 2012.

[15] H. L. Van Trees, *Optimum Array Processing*. New York: Wiley-Interscience, 2002. [Online]. Available: http://opac.inria.fr/record=b1105852

[16] J. Li and P. Stoica, *MIMO Radar Signal Processing*. John Wiley & Sons, Inc., Hoboken, NJ, 2009.

[17] A. Papoulis and S. U. Pillai, *Probability, Random Variables, and Stochastic Processes*, 4th ed. McGraw-Hill Higher Education, 2002.

[18] S. Kay, *Fundamentals of Statistical Signal Processing: Detection theory*, ser. Prentice Hall Signal Processing Series. Prentice-Hall PTR, 1998. [Online]. Available: https://books.google.co.uk/books?id=vA9LAQAAIAAJ

[19] M. Arulampalam, S. Maskell, N. Gordon, and T. Clapp, "A tutorial on particle filters for online nonlinear/non-gaussian bayesian tracking," *Signal Processing, IEEE Transactions on*, vol. 50, no. 2, pp. 174–188, Feb 2002.

[20] W. H. Press, S. A. Teukolsky, W. T. Vetterling, and B. P. Flannery, *Numerical Recipes in C (2Nd Ed.): The Art of Scientific Computing*. New York, NY, USA: Cambridge University Press, 1992.